



HAL
open science

Structure of bacteriophage SPP1 head-to-tail connection reveals mechanism for viral DNA gating

Sophie Lhuillier, Matthieu Gallopin, Bernard Gilquin, Sandrine Brasilès, Nathalie Lancelot, Guillaume Letellier, Mathilde Gilles, Guillaume Dethan, Elena V. Orlova, Joël Couprie, et al.

► To cite this version:

Sophie Lhuillier, Matthieu Gallopin, Bernard Gilquin, Sandrine Brasilès, Nathalie Lancelot, et al.. Structure of bacteriophage SPP1 head-to-tail connection reveals mechanism for viral DNA gating. Proceedings of the National Academy of Sciences of the United States of America, 2009, 106 (21), pp.8507-8512. 10.1073/pnas.0812407106 . hal-02662470

HAL Id: hal-02662470

<https://hal.inrae.fr/hal-02662470>

Submitted on 31 May 2020

HAL is a multi-disciplinary open access archive for the deposit and dissemination of scientific research documents, whether they are published or not. The documents may come from teaching and research institutions in France or abroad, or from public or private research centers.

L'archive ouverte pluridisciplinaire **HAL**, est destinée au dépôt et à la diffusion de documents scientifiques de niveau recherche, publiés ou non, émanant des établissements d'enseignement et de recherche français ou étrangers, des laboratoires publics ou privés.

Structure of bacteriophage SPP1 head-to-tail connection reveals mechanism for viral DNA gating

Sophie Lhuillier^a, Matthieu Gallopin^b, Bernard Gilquin^b, Sandrine Brasilès^a, Nathalie Lancelot^b, Guillaume Letellier^b, Mathilde Gilles^b, Guillaume Dethan^b, Elena V. Orlova^c, Joël Couprie^b, Paulo Tavares^{a,1}, and Sophie Zinn-Justin^{b,1}

^aUnité de Virologie Moléculaire et Structurale, Centre National de la Recherche Scientifique, Unité Mixte de Recherche 2472, Institut National de la Recherche Agronomique, Unité Mixte de Recherche 1157 and Institut Fédératif de Recherche 115, Bât. 14B, Centre National de la Recherche Scientifique, 91198 Gif-sur-Yvette, France; ^bLaboratoire de Biologie Structurale et Radiobiologie, iBiTec-5 et Centre National de la Recherche Scientifique URA2096, Bât. 144, Commissariat à l'Energie Atomique, Saclay, 91191 Gif-sur-Yvette, France; and ^cSchool of Crystallography, Birkbeck College, Malet Street, London WC1E 7HX, United Kingdom

Edited by Michael G. Rossmann, Purdue University, West Lafayette, IN, and approved March 5, 2009 (received for review December 5, 2008)

In many bacterial viruses and in certain animal viruses, the double-stranded DNA genome enters and exits the capsid through a portal gatekeeper. We report a pseudoatomic structure of a complete portal system. The bacteriophage SPP1 gatekeeper is composed of dodecamers of the portal protein gp6, the adaptor gp15, and the stopper gp16. The solution structures of gp15 and gp16 were determined by NMR. They were then docked together with the X-ray structure of gp6 into the electron density of the \approx 1-MDa SPP1 portal complex purified from DNA-filled capsids. The resulting structure reveals that gatekeeper assembly is accompanied by a large rearrangement of the gp15 structure and by folding of a flexible loop of gp16 to form an intersubunit parallel β -sheet that closes the portal channel. This stopper system prevents release of packaged DNA. Disulfide cross-linking between β -strands of the stopper blocks the key conformational changes that control genome ejection from the virus at the beginning of host infection.

NMR | structure docking | unstructured proteins | virus assembly | virus infection

Virus particles are designed to protect the viral genome and to ensure its efficient delivery to the host cell. During assembly of a large number of viruses such as bacteriophages (1–5) and herpesviruses (6), double-stranded DNA (dsDNA) is actively transported through the central channel of the portal protein into the interior of the procapsid (Fig. 1A). The reaction fuelled by a viral packaging ATPase leads to a dense packing of dsDNA. The concentrations reached (\approx 500 mg/mL) can apply pressures \approx 6 MPa in the capsid lattice (7–9). Packaging termination is coordinated with closure of the portal channel to avoid leakage of the highly compacted nucleic acid. In tailed bacteriophages, this can be achieved by a conformational change in the portal protein structure (10, 11) or by binding of head completion proteins that close the portal channel forming the connector (2, 4, 12–15). Precisely, the connector is defined as the knob structure at the capsid portal vertex where the bacteriophage tail attaches (2) (Fig. 1A). Note that some authors use the term connector as synonymous with portal protein (5, 10, 12) rather than to designate the complete structure assembled at the portal vertex of the capsid structure. Closure of the portal channel within the connector complex is reversed to allow DNA release from the phage capsid, a requirement for viral genome delivery to the bacterial cytoplasm at the beginning of host cell infection.

Bacillus subtilis bacteriophage SPP1 is a paradigm for viruses with a portal system (1). It is a 45.1-kbp-long dsDNA virus (9) with an isometric capsid of \approx 60-nm diameter and a 191-nm-long noncontractile tail (16). The SPP1 head-to-tail connector is composed of cyclical dodecamers of the portal protein gp6 (subunit molecular mass of 57.3 kDa) and of the 2 head completion proteins gp15 (11.6 kDa) and gp16 (12.5 kDa) (2, 17) (Fig. 1A). Gp6 asymmetric position in the procapsid defines the portal vertex. Its central channel provides the path for genome

packaging during SPP1 assembly. Binding of gp15 and gp16 to the portal protein after encapsidation is essential to avoid leakage of packaged DNA (2). The DNA extremity that is packaged last remains attached to the connector. A 19- to 29-nm segment of the SPP1 genome is protected by this structure in the phage particle (18). The gp16 ring provides the interface for phage tail attachment, the step that ends phage assembly. Infection is initiated by binding of SPP1 to the surface of the Gram-positive host bacterium. Interaction of the phage tail adsorption apparatus with the receptor YueB generates a signal transmitted along the tail structure to trigger opening of the connector (16, 19). Its aperture leads to DNA exit from the capsid through the tail tube to reach the *B. subtilis* cytoplasm (19).

The program of head completion proteins conformational changes leading to connector assembly at the portal vertex and the molecular basis of their gating function in phage genome release remain unknown. To address these questions, we determined the first pseudoatomic structure of a complete genome gatekeeper. Structures of SPP1 gp15 and gp16 monomers were determined by NMR and docked together with the available X-ray structure of gp6 (20) into the cryo-EM reconstruction of the connector purified from DNA-filled capsids (2). Comparison of the structures before and after assembly provide details on major structural rearrangements (gp15) and folding events (gp15 and gp16) that accompany connector formation. Of particular importance is folding of a gp16 loop into a putative β -strand that forms a parallel intersubunit β -sheet closing the central channel of the gp16 dodecamer. Unzipping of the β -sheet is shown to be an essential step of the mechanism of nucleocapsid gatekeeper opening for DNA release from the virus particle.

Results

Solution Structures of the α -Helical gp15 and the β -Stranded gp16 Monomers. We have determined the solution structures of both gp15 and gp16 monomers by NMR [Fig. 1B and D, supporting information (SI) Fig. S1A, and Tables S1 and S2]. Gp15 forms a well-defined 3- α -helix bundle decorated by an N-terminal helix α 0, a small β -hairpin, and a large poorly structured loop between α 2 and α 3 (from T66 to S88; Fig. 1B). The relative positions of the helices of the bundle are stabilized by hydrophobic contacts between: (i) L21, V25, and V29 on α 1 and V53, V57, and A61

Author contributions: J.C., P.T., and S.Z.-J. designed research; S.L., M. Gallopin, B.G., S.B., N.L., G.L., M. Gilles, G.D., and J.C. performed research; S.L., M. Gallopin, B.G., E.V.O., and J.C. analyzed data; and P.T. and S.Z.-J. wrote the paper.

The authors declare no conflict of interest.

This article is a PNAS Direct Submission.

See Commentary on page 8403.

¹To whom correspondence may be addressed. E-mail: sophie.zinn@cea.fr or tavares@vms.cnrs-gif.fr.

This article contains supporting information online at www.pnas.org/cgi/content/full/0812407106/DCSupplemental.

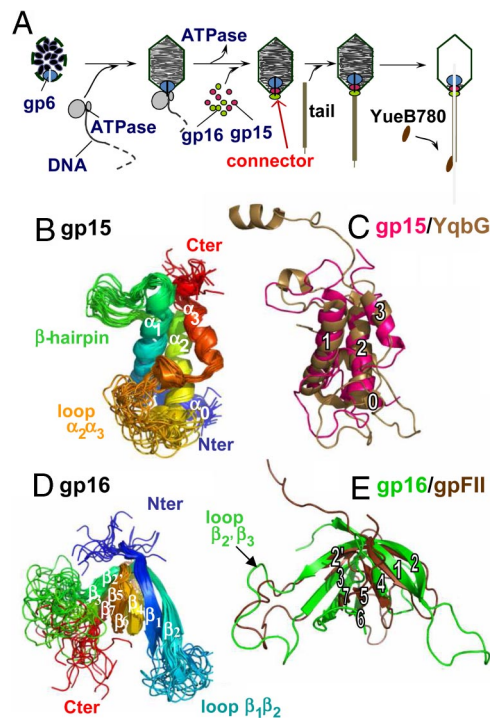


Fig. 1. Structure of bacteriophage SPP1 head completion proteins. (A) Connector proteins (gp6, gp15, and gp16) are identified within the SPP1 assembly and DNA ejection pathway. YueB780 is the ectodomain of *B. subtilis* YueB, the SPP1 receptor. (B) Superimposition of 20 backbone structures of gp15 (residues 4 to 102; PDB ID code 2KBZ) solved by NMR at pH 6.5 and 22 °C. The backbone rmsd relative to the mean structure calculated on the α -helix bundle yields 0.5 ± 0.1 Å. Ribbons are colored from blue (N terminus) to red (C terminus). (C) Superimposition of gp15 (magenta) and YqbG from the skin prophage-like element of *B. subtilis* (PDB ID code 1XN8; brown). (D) Structures of gp16 (residues 2–109; PDB ID code 2KCA) solved by NMR at pH 6.5 and 37 °C. The backbone rmsd relative to the mean structure calculated on the β -barrel yields 0.9 ± 0.3 Å. Ribbons are colored from blue (N terminus) to red (C terminus). (E) Superimposition of gp16 (green) and gpFII from phage λ (PDB ID code 1K0H; brown).

on $\alpha 2$, respectively; (ii) L28 and A32 on $\alpha 1$ and L91 and L94 on $\alpha 3$; (iii) F56 and A60 on $\alpha 2$ and I90 on $\alpha 3$. $^1\text{H} \rightarrow ^{15}\text{N}$ nOe experiments show the high mobility of the loop $\alpha 2\alpha 3$ on the picosecond-to-nanosecond time scale (Fig. S1B). A DALI search for structural analogs of gp15 highlighted YqbG encoded by the prophage-like element of *B. subtilis* named skin (21) (Fig. 1C and Fig. S2A). Detailed comparison of gp15 and YqbG topologies shows that positioning of the large loop $\alpha 2\alpha 3$ and the β -hairpin relative to the α -helix bundle is remarkably conserved (backbone rmsd of YqbG relative to the gp15 structures: 1.9 ± 0.2 Å). GpW from bacteriophage λ is a functional analog of gp15. This polypeptide interacts both with the portal protein gpB and with the head completion protein gpFII (22, 23) of λ . GpW exhibits 2 large α -helices separated by a β -hairpin (23) as gp15 and YqbG (Fig. S2C). However, the angle between the 2 large helices and the side of the helices where the β -hairpin interacts are different. Moreover, gpW lacks the additional N- and C-terminal α -helices exhibited by gp15 and YqbG. Thus, gpW and gp15/YqbG represent 2 distinct folds designed to accomplish similar biological functions.

The structure of SPP1 gp16 reveals a well-defined β -barrel that is flanked by 2 long unstructured loops $\beta 1\beta 2$ and $\beta 2'\beta 3$ (Fig. 1D). The barrel is constituted by 2 β -sheets $\beta 1/\beta 2/\beta 4/\beta 5$ and $\beta 2'/\beta 3/\beta 7/\beta 6$, the β -strands $\beta 2$, $\beta 2'$ and $\beta 5$, $\beta 6$ being contiguous in several structures. Its backbone is stable after 6 ns of molecular dynamics in explicit water, whereas the 2 loops are

highly mobile on a picosecond-to-nanosecond time scale (Fig. S3). The gp16 β -barrel fold is reminiscent of that described for the head completion protein gpFII of phage λ (24), a functional analog of gp16 (Fig. 1E). Their common topology consists of a first β -sheet formed by β -strands $\beta 1$, $\beta 2$, $\beta 4$, $\beta 5$ extended by $\beta 6$ ($\beta 5$ and $\beta 6$ form a continuous β -strand in gpFII), and $\beta 7$ and a second β -sheet limited to $\beta 2'$ and $\beta 3$ ($\beta 3$ forms a β -sheet with $\beta 7$ in gp16). This structural similarity allows a straightforward alignment between the poorly related sequences of gp16 and gpFII (Fig. S4A). The length of the loops spacing the β -strands is different in the 2 polypeptides. The only exception is the largest loop located between strands $\beta 2'$ and $\beta 3$ that consists of 19 residues in both proteins. Sequence alignment of 26 phage proteins >25% identical to gp16 shows that the length of loop $\beta 2'\beta 3$ is also conserved within these polypeptides (Fig. S4B).

Docking of gp15 and gp16 Structures into the Electron Microscopy Density of the SPP1 Connector. The sets of NMR structures of gp15 and gp16 that provide a sampling of each protein's conformational landscape were docked into the 10-Å resolution cryoEM reconstruction of the closed connector found in viral capsids (2). In case of gp15, simultaneous positioning of the large helices $\alpha 1$ and $\alpha 2$ into the EM density of the gp15 ring was not possible, revealing that it undergoes a structural rearrangement during connector assembly. Normal mode analysis (25) identified the loop between the β -hairpin and $\alpha 2$ as the most probable hinge region in the molecule. Each of the 20 gp15 NMR lowest-energy structures was dissected into 2 segments separated by the hinge ($\alpha 0 + \alpha 1 + \beta$ -hairpin and $\alpha 2 + \alpha 3$). These segments were simultaneously docked into the EM density of the gp15 ring. Thirteen similar dodecameric models were obtained that fit well the EM density and maintain the 2 segments connected without disrupting the β -hairpin between helices $\alpha 1$ and $\alpha 2$ (Fig. 2A and Table S3). The conformation adopted by gp15 implies that its N-terminal segment undergoes a motion of 15.4 ± 2.1 Å relative to the C-terminal segment (Fig. 2A and Table S3). Disruption of the $\alpha 1$ - $\alpha 2$ interface is stabilized by intercalation of $\alpha 0$ from the adjacent subunit between the 2 large helices during gp15 oligomerization at the portal vertex. The conformation of assembled gp15 also implies that its amino terminus points toward the gp16 dodecamer (Fig. 2A). This explains how a hexahistidine insertion at the gp15 N terminus allows for gp6 binding but impairs interaction with gp16 during connector formation. The gp15 interface exposed to gp16 is highly basic (Fig. 3A).

Rigid-body docking of the 10 lowest-energy gp16 conformers into the corresponding ring of the connector EM map (2) resulted in 10 dodecamer models that fit very well the EM density [cross-correlation (Cc)-values between 59.7 and 67.5 at 10 Å]. In 3 similar dodecameric structures, loop $\beta 2'\beta 3$ is positioned in the stopper region closing the central connector channel (Table S4). The loop mass fills particularly well the 1.6 kDa contributed by each individual gp16 subunit to the stopper mass. Moreover, only loop $\beta 2'\beta 3$ presents no insertion or deletion within gpFII and the 26 polypeptides analogous to gp16, supporting a functional role for its conserved length (Fig. S4). Because this loop is poorly structured in free gp16, we calculated loop $\beta 2'\beta 3$ structures that would fit the EM density of the stopper using a simulated annealing protocol. The envelope of the density was represented by many partially overlapping spheres, and several distances were restrained between loop $\beta 2'\beta 3$ residues and the spheres during loop structure calculation (26). The model of the stopper region in which the steric clashes among the 12 loops are minimal is shown in Figs. 2B, 4A and B, and 5A. Each subunit contributes to the stopper through a β -strand Q43-Q51, which forms parallel β -sheets with the β -strands of contiguous subunits.

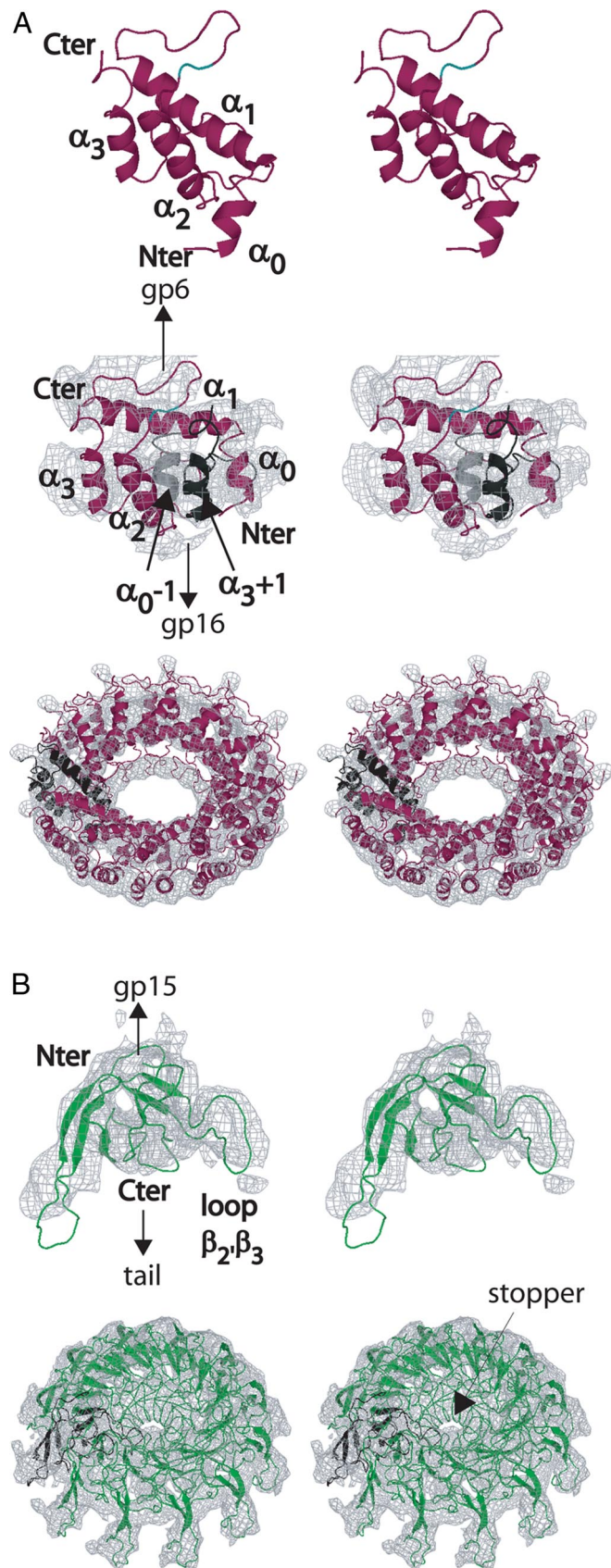


Fig. 2. Docking of gp15 and gp16 structures in the SPP1 connector reconstruction (stereo views). (A) Displacement of the gp15 N-terminal fragment (helices α_0 and α_1 and the β -hairpin) relative to its C-terminal fragment (helices α_2 and α_3) during connector assembly. The gp15 NMR structure is

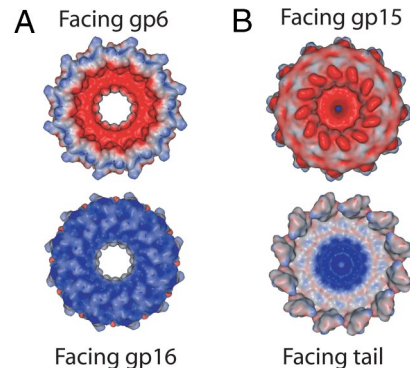


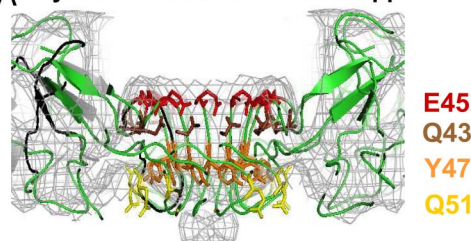
Fig. 3. Gp15 and gp16 dodecamers electrostatic potential surfaces calculated with PBEQ-Solver (38). Colored from red (negative) to blue (positive). (A) Gp15 surface as viewed from gp6 (Upper) and gp16 (Lower). (B) Gp16 surface as viewed from gp15 (Upper) and the tail (Lower).

Engineering of Disulfide Intersubunit Bridges Between Stopper Parallel β -Strands and DNA Ejection Through the SPP1 Connector. Positioning of the large loop $\beta_2'\beta_3$ in the stopper region identified the gp16 region that closes the connector channel and controls DNA exit from the viral capsid. Formation of a parallel intersubunit β -sheet in the stopper implies that residues at identical positions in loop $\beta_2'\beta_3$ align with their counterparts from adjacent subunits. Residues C α are distanced by 5 Å, and lateral chains are side-by-side in the assembled connector (Fig. 5A). These features are compatible with formation of disulfide bridges between cysteines in adjacent β -strands (27). We have thus used disulfide cross-linking to study stopper assembly and its opening for DNA release. Single cysteine substitutions of residues Q43, E45, Y47, or Q51 in loop $\beta_2'\beta_3$ (Fig. 5A) lead to no detectable intersubunit cross-linking of unassembled gp16 consistent with its monomeric state (Fig. 5B). In contrast, disulfide-linked gp16 dimers are formed in the connector of phages carrying mutations E45C, Y47C, or Q51C (upper bands in Fig. 5C). Note that higher-order cross-linked species (e.g., trimer) cannot be formed because each gp15 subunit has a single cysteine that allows making a disulfide bond with only 1 of its 2 neighbor subunits in the gp15 dodecamer. Complete intersubunit cross-linking is found in case of the gp16 double mutant Q43CQ51C, where the stopper β -sheet can be stabilized by combination of 2 different types of disulfide bridges (C43-C43₊₁ or C43-C43₋₁ and C51-C51₊₁ or C51-C51₋₁) (Fig. 5A and C). In this mutant, a minor population of gp15 cross-linked trimers is detected in overexposed Western blot analyses, revealing that combination of C43-C43₊₁ with C51-C51₋₁ or C43-C43₋₁ with C51-C51₊₁ disulfide bridges can be formed albeit with low frequency. No higher-order cross-linked species were found in assembled gp16_{Q43CQ51C}.

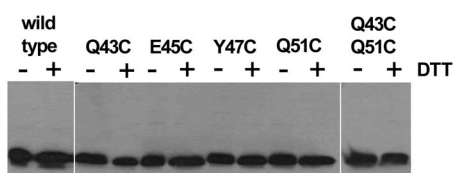
We then investigated the effect of covalent intersubunit cross-linking of the stopper in viral genome ejection using a DNase protection assay that quantifies nonejected DNA (9, 19).

shown (Top), and gp15 docked into the connector EM density is shown (Middle). Both structures are colored in magenta. The hinge residues are colored in cyan. In Middle, helix α_0 of the neighbor subunit on the left is shown in gray, and helix α_3 of the adjacent subunit on the right is shown in black. Note that the distance between the C terminus of helix α_1 and the N terminus of helix α_2 does not vary during docking ensuring that the central β -hairpin between helices α_1 and α_2 is not disrupted. (Bottom) A tilted top view of the gp15 dodecamer model is shown beneath the docking of the individual subunit. Helix α_1 is in the EM density close to gp6, helices α_2 and α_3 are in the outer part, and loop α_2 - α_3 is in the inner ring of the connector close to gp16. (B) Docking of the gp16 monomer structure as a rigid body in the connector EM map of the gp16 ring (Upper) and model of the gp16 dodecamer (Lower). The N terminus, loop $\beta_2\beta_2'$, loop $\beta_3\beta_4$, and loop $\beta_6\beta_7$ are located close to gp15, whereas loop $\beta_2'\beta_3$ fills the stopper EM density on the tail side.

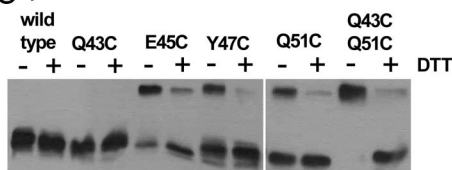
A cysteine mutations in the stopper



B extracts of *B. subtilis* producing gp16 from a plasmid



C purified virions



D DNA ejection from virions (DNase protection assay)

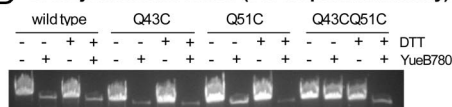


Fig. 5. Gp16 intersubunit disulfide bonding of the stopper region and DNA ejection. (A) Structure of the gp16 stopper. Residues mutated to cysteine are identified by colors. (B and C) Effect of stopper amino acid substitutions to cysteine in monomeric gp16 (B; no cross-linking) and in its dodecameric assembled form found in viral particles (C; formation of covalently bound subunit dimers (upper bands) in oxidation conditions that were efficiently reduced with 4 mM DTT). (D) DNA ejection from virions bearing gp16 mutations was assayed by a DNase protection method that reveals the amount of DNA not released from viral particles (19). Ejection was triggered by receptor addition using a ratio of 1,250 YueB780 dimers (19) per virion in the presence and in the absence of 4 mM DTT. All results were reproduced in at least 3 independent experiments.

pseudoatomic structure presented here is found in DNA-filled capsids (Fig. 1A) (2). Gp16 opening for DNA to enter the tail tube could occur either upon tail attachment to capsids (30) or in response to signaling through the tail tube after virions binding to the bacterial receptor (16) (Fig. 1A). The impact of tail binding on gp16 conformation is unknown at present. However, we note that no disulfide bridges are formed in the reducing environment of the bacterial cytoplasm during morphogenesis *in vivo* of phages carrying gp16 cysteine mutants. Thus, the gp16 stopper could open normally for DNA to enter the tail after tail assembly. When phages are released from infected cells, disulfide bridges form in gp16 upon cysteine oxidation in the presence of environmental oxygen. If the gp16 stopper were already open at the end of phage assembly, no blockage of DNA ejection would be expected from gp16 intersubunit disulfide cross-linking. The inhibitory effect observed (Fig. 5D) suggests that it is receptor binding to the phage that initiates a signal leading to the conformational change in the stopper necessary for viral genome release.

We propose that the general role of the bacteriophage stopper protein is to keep DNA in the head before the tail attaches and to control the exit of DNA from the capsid at the beginning of

viral infection. The stopper could also participate in DNA binding. Indeed, during connector assembly, gp16 is appropriately positioned to bind the DNA end that is found attached to the connector in phage particles (18). In SPP1, stabilization of this interaction requires binding of the tail to the connector (17). Several factors thus contribute to DNA association with the connector. This might explain why substitution K48E in gp16 does not have a profound effect in phage viability in spite of the fact that K48 forms a ring of lysines in the most constricted region of the stopper, making a major contribution to its electropositive potential (Fig. 3B). Further work will highlight the details of the connector–DNA interaction and the stopper intersubunit β -sheet unzipping events that lead to connector opening with concomitant genome passage to reach the bacterial cytoplasm.

Methods

Cloning and Site-Directed Mutagenesis. Cloning in plasmids for production of different versions of gp15 and gp16 was carried out by using PCR procedures and their biological activity assayed by complementation assays *in vivo* (SI Materials and Methods and Table S5).

Protein Production and Purification. N terminus-tagged gp15 (H15) and gp16 (H16) (17) were overproduced in M9 medium containing $(^{15}\text{NH}_4)_2\text{SO}_4$ (Cambridge Isotope Laboratories) as the only nitrogen source or in medium containing ^{13}C -glucose (Cambridge Isotope Laboratories) and $(^{15}\text{NH}_4)_2\text{SO}_4$ to obtain ^{15}N - or $^{15}\text{N}^{13}\text{C}$ -labeled protein, respectively. H16 was also produced during 18–20 h at 37 °C in M9 medium with 98% D_2O (CEA) in a ^{13}C -glucose- and $(^{15}\text{NH}_4)_2\text{SO}_4$ -enriched medium to obtain a $^{15}\text{N}^{13}\text{C}^2\text{H}$ -labeled protein. In all cases, the bacterial pellets were resuspended in 300 mM NaCl, 50 mM Hepes, and 50 mM imidazole (pH 8). H15 and H16 were purified by affinity chromatography on a HiTrap metal chelating HP column (GE Healthcare), and the tagged protein peak was immediately applied to a size-exclusion chromatography column (Sephadex S75 26/60; GE Healthcare) equilibrated with 300 mM NaCl, 5 mM Hepes, and 1 mM EDTA (pH 6.5). Proteins were concentrated by ultracentrifugation in vivaspin 5000 (Vivascience) up to 6–20 mg/mL.

Strain BL21(DE3) (pSB111) coding for the gp15-intein/chitin binding domain fusion protein was grown in medium M9 containing $(^{15}\text{NH}_4)_2\text{SO}_4$ supplemented with 100 $\mu\text{g}/\text{mL}$ ampicillin at 37 °C. Bacteria were induced with 0.3 mM IPTG after reaching a density of $\approx 10^8$ cfu/mL and further incubated for 3 h at 20 °C. Sedimented bacteria were resuspended in intein buffer [500 mM NaCl, 1 mM EDTA, 20 mM Hepes (pH 7.5)] supplemented with a mixture of proteases inhibitor (Roche) and lysed by sonication. The crude extract was applied to a column of chitin beads (New England Biolabs) that was washed with 10 volumes of intein buffer. Autocleavage of the intein-gp15 fusion protein was carried out overnight with 50 mM DTT in the closed column followed by elution of gp15 with intein buffer.

NMR Spectroscopy and Structure Calculation. Most NMR experiments were recorded on Bruker 600- and 700-MHz spectrometers equipped with a triple resonance cryoprobe (Saclay). Additional NMR experiments were performed on the 750-MHz Bruker spectrometer of the European Facility in Utrecht, The Netherlands, and on the Varian 800-MHz spectrometer of the National Facility in Grenoble, France. For H16, in addition to the classical 3D heteronuclear experiments recorded on ^{15}N - and $^{15}\text{N}^{13}\text{C}$ -labeled samples, HNCACB, HNCACO, and HNCOCACB experiments were recorded on a $^{15}\text{N}^{13}\text{C}^2\text{H}$ -labeled sample. All NMR spectra were processed with the programs Xwinnmr (Bruker) or NMRPipe (31) and analyzed by using Sparky (T.D. Goddard and D.G. Kneller, University of California, San Francisco). H15 and H16 backbone assignment (SI Materials and Methods) was facilitated by the use of the program MARS (32). The program TALOS (33) allowed determination of the ϕ, ψ angles on the basis of the analysis of the $^{13}\text{C}_\alpha$, $^{13}\text{C}_\beta$, $^{13}\text{C}_\gamma$, $^1\text{H}_\alpha$, and ^{15}N chemical shifts. ^1H - ^{15}N HSQC spectra of tag-free gp15 were recorded and compared with spectra of H15 obtained under identical conditions (Fig. S1A). Solution structure calculations were carried out by using INCA (34) and CNS (35) (Tables S1 and S2 and Fig. S5 A and B). Molecular dynamics simulations were performed on the energetically most-favorable gp15 and gp16 models positioned in a water box of $85 \times 85 \times 85 \text{ \AA}$ during 6–10 ns (Table S2 and Fig. S5C). For these calculations, the simulator was NAMD2 and the force field Charmm27.

Docking of NMR Structures into EM Maps. First, a model of the gp6 dodecamer (20) was fitted into the EM map of the SPP1 connector [EBI reference: EMD-1021 (2)] at a resolution of 10 \AA to validate the estimated value of the

EMD.1021 map pixel in angstroms. An optimal value of 1.9 Å per pixel was found by UROX (36). To position the gp15 NMR structures into the EM density of the connector, we first extracted the EM map corresponding to the gp15 dodecamer (2). Fitting of each of the 20 gp15 NMR structures into this EM map was performed manually and optimized by using UROX. This procedure did not lead to any acceptable solution at a resolution of 10 Å. The HingeMaster server (25) was then used to predict the position of hinges around which the gp15 structure could bend during its assembly into the connector. The normal mode motion correlation based method hNMB proposed the loop between the β -hairpin and $\alpha 2$ as the most probable hinge region in gp15. A second round of docking trials was carried out by fitting independently segment 4–50 (comprising $\alpha 0$, $\alpha 1$, $\beta 1$, and $\beta 2$) and segment 51–102 (comprising $\alpha 2$ and $\alpha 3$) (Fig. 2A) yielding 1 family of 13 similar dodecameric structures in which the 2 gp15 fragments are connected (variation of the C_{α} distance between residues 36 and 51 relative to the native structure is <3 Å; Table S3) and fit well into the EM maps.

In the case of gp16, each NMR structure was manually positioned by fitting the large sheet $\beta 1\beta 2$ into 1 of the 12 “feet” of the EM density assigned to the gp16 dodecamer (Fig. 2B). UROX was then used for calculation of a preliminary model of the dodecameric particle and for optimization of the subunit position in the EM map. Adjustments were successively calculated at resolutions of 40, 30, 20, 15, and 10 Å to explore the docking possibilities. Features of the 10 resulting gp16 dodecameric pseudoatomic models are compiled in

Table S4 and in Fig. 2B. Modeling of loop $\beta 2'\beta 3$ structures fitting the EM density of the stopper was carried out by using CNS (35).

Finally, to position gp16, gp15, and gp6 structures into the connector EM density, UROX was applied simultaneously on the 3 dodecamers obtained from the previous UROX adjustments of the individual proteins.

Disulfide Bridges and DNA Ejection Assays. Strains bearing plasmids coding for gp16 mutant proteins were infected with SPP1*sus117* (2) to produce phages carrying different gp16 cysteine substitutions. CsCl-purified phages and *B. subtilis* extracts of gp16-producing strains were used as sources of assembled and of free gp16 mutant proteins, respectively. Formation of intersubunit disulfide bridges and their reduction with 4 mM DTT followed by alkylation with 10 mM NEM were analyzed as described (37). DNA ejection triggered with YueB780 was assayed by using a DNase [Benzonase; (Merck)] protection assay previously described (9, 19).

ACKNOWLEDGMENTS. J. Lepault is acknowledged for useful explanations and discussions. We thank J. B. Charbonnier, R. Guérois, and H. Saibil for critical reading of the manuscript. Access to the EU-NMR facility of Utrecht supported by the 6th Framework Programme of the EC (Contract #RII3-026145, EU-NMR) and the RALF-NMR national facility of Grenoble is gratefully acknowledged. The work was supported by Commissariat à l’Energie Atomique institutional funding (to S.Z.-J.), and Centre National de la Recherche Scientifique institutional Grants ATIP and ANR-06-BLAN-0168 (to P.T.)

- Catalano CE (2005) *Viral Genome Packaging: Genetics, Structure, and Mechanism* (Springer, New York).
- Orlova EV, et al. (2003) Structure of a viral DNA gatekeeper at 10 Å resolution by cryo-electron microscopy. *EMBO J* 22:1255–1262.
- Gowen B, Bamford JK, Bamford DH, Fuller SD (2003) The tailless icosahedral membrane virus PRD1 localizes the proteins involved in genome packaging and injection at a unique vertex. *J Virol* 77:7863–7871.
- Jiang W, et al. (2006) Structure of epsilon15 bacteriophage reveals genome organization and DNA packaging/injection apparatus. *Nature* 439:612–616.
- Xiang Y, et al. (2006) Structural changes of bacteriophage phi29 upon DNA packaging and release. *EMBO J* 25:5229–5239.
- Newcomb WW, Booy FP, Brown JC (2007) Uncoating the herpes simplex virus genome. *J Mol Biol* 370:633–642.
- Smith DE, et al. (2001) The bacteriophage $\phi 29$ portal motor can package DNA against a large internal force. *Nature* 413:748–752.
- Evilleitch A, Lavelle L, Knobler CM, Raspaud E, Gelbart WM (2003) Osmotic pressure inhibition of DNA ejection from phage. *Proc Natl Acad Sci USA* 100:9292–9295.
- São-José C, de Frutos M, Raspaud E, Santos MA, Tavares P (2007) Pressure built by DNA packing inside virions: Enough to drive DNA ejection in vitro, largely insufficient for delivery into the bacterial cytoplasm. *J Mol Biol* 374:346–355.
- Donate LE, et al. (1988) Bacteriophage T3 connector: Three-dimensional structure and comparison with other viral head-tail connecting regions. *J Mol Biol* 201:91–100.
- Valpuesta JM, Fujisawa H, Marco S, Carazo JM, Carrascosa JL (1992) Three-dimensional structure of T3 connector purified from overexpressing bacteria. *J Mol Biol* 224:103–112.
- Coombs DH, Eiserling FA (1977) Studies on the structure, protein composition and assembly of the neck of bacteriophage T4. *J Mol Biol* 116:375–405.
- Perucchetti R, Parris W, Becker A, Gold M (1988) Late stages in bacteriophage lambda head morphogenesis: In vitro studies on the action of the bacteriophage lambda D-gene and W-gene products. *Virology* 165:103–114.
- Strauss H, King J (1984) Steps in the stabilisation of newly packaged DNA during phage P22 morphogenesis. *J Mol Biol* 172:523–543.
- Zheng H, et al. (2008) A conformational switch in bacteriophage p22 portal protein primes genome injection. *Mol Cell* 29:376–383.
- Plisson C, et al. (2007) Structure of bacteriophage SPP1 tail reveals trigger for DNA ejection. *EMBO J* 26:3720–3728.
- Lurz R, et al. (2001) Structural organisation of the head-to-tail interface of a bacterial virus. *J Mol Biol* 310:1027–1037.
- Tavares P, Lurz R, Stiege A, Rückert B, Trautner TA (1996) Sequential headful packaging and fate of the cleaved DNA ends in bacteriophage SPP1. *J Mol Biol* 264:954–967.
- São-José C, et al. (2006) The ectodomain of the viral receptor YueB forms a fiber that triggers DNA ejection of bacteriophage SPP1 DNA. *J Biol Chem* 281:11464–11470.
- Lebedev AA, et al. (2007) Structural framework for DNA translocation via the viral portal protein. *EMBO J* 26:1984–1994.
- Kunst F, et al. (1997) The complete genome sequence of the Gram-positive bacterium *Bacillus subtilis*. *Nature* 390:249–256.
- Maxwell KL, Davidson AR, Murialdo H, Gold M (2000) Thermodynamic and functional characterization of protein W from bacteriophage lambda. The three C-terminal residues are critical for activity. *J Biol Chem* 275:18879–18886.
- Maxwell KL, et al. (2001) The solution structure of bacteriophage lambda protein W, a small morphogenetic protein possessing a novel fold. *J Mol Biol* 308:9–14.
- Maxwell KL, Yee AA, Arrowsmith CH, Gold M, Davidson AR (2002) The solution structure of the bacteriophage lambda head-tail joining protein, gpFII. *J Mol Biol* 318:1395–1404.
- Flores SC, et al. (2008) HingeMaster: Normal mode hinge prediction approach and integration of complementary predictors. *Proteins* 73:299–319.
- Alber F, et al. (2007) The molecular architecture of the nuclear pore complex. *Nature* 450:695–701.
- Matsumura M, Bechtel WJ, Levitt M, Matthews BW (1989) Stabilization of phage T4 lysozyme by engineered disulfide bonds. *Proc Natl Acad Sci USA* 86:6562–6566.
- Isidro A, Henriques AO, Tavares P (2004) The portal protein plays essential roles at different steps of the SPP1 DNA packaging process. *Virology* 322:253–263.
- Dyson JH, Wright PE (2005) Intrinsically unstructured proteins and their functions. *Nat Rev Mol Cell Biol* 6:197–208.
- Thomas JO (1974) Chemical linkage of the tail to the right-hand end of bacteriophage lambda DNA. *J Mol Biol* 87:1–9.
- Delaglio F, et al. (1995) NMRPipe: A multidimensional spectral processing system based on UNIX pipes. *J Biomol NMR* 6:277–293.
- Jung YS, Zweckstetter M (2004) Mars—robust automatic backbone assignment of proteins. *J Biomol NMR* 30:11–23.
- Cornilescu G, Delaglio F, Bax A (1999) Protein backbone angle restraints from searching a database for chemical shift and sequence homology. *J Biomol NMR* 13:289–302.
- Savarin P, Zinn-Justin S, Gilquin B (2001) Variability in automated assignment of NOESY spectra and three-dimensional structure determination: A test case on three small disulfide-bonded proteins. *J Biomol NMR* 19:49–62.
- Brünger AT (2007) Version 1.2 of the Crystallography and NMR System. *Nat Protocols* 2:2728–2733.
- Navaza J, Lepault J, Rey FA, Álvarez-Rúa C, Borge J (2002) On the fitting of model electron densities into EM reconstructions: A reciprocal-space formulation. *Acta Crystallogr D* 58:1820–1825.
- Cuervo A, Vaney MC, Antson AA, Tavares P, Oliveira L (2007) Structural rearrangements between portal protein subunits are essential for viral DNA translocation. *J Biol Chem* 282:18907–18913.
- Jo S, Vargyas M, Vasko-Szedlar J, Roux B, Im W (2008) PBEQ-solver for online visualization of electrostatic potential of biomolecules. *Nucleic Acids Res* 36:W270–W275.